

Article

A Model-Based Sensor Fault Diagnosis Scheme for Batteries in Electric Vehicles

Quanqing Yu ^{1,2} , Changjiang Wan ¹, Junfu Li ¹, Rui Xiong ^{2,*}  and Zeyu Chen ³

¹ School of Automotive Engineering, Harbin Institute of Technology, Weihai 264209, China; qqyu@hit.edu.cn (Q.Y.); wcjst@outlook.com (C.W.); lijunfu@hit.edu.cn (J.L.)

² National Engineering Laboratory for Electric Vehicles, School of Mechanical Engineering, Beijing Institute of Technology, Beijing 100081, China

³ School of Mechanical Engineering and Automation, Northeastern University, Shenyang 110819, China; chenzy@mail.neu.edu.cn

* Correspondence: rxiong@bit.edu.cn; Tel.: +86-(10)-6891-6608

Abstract: The implementation of each function of a battery management system (BMS) depends on sensor data. Efficient sensor fault diagnosis is essential to the durability and safety of battery systems. In this paper, a model-based sensor fault diagnosis scheme and fault-tolerant control strategy for a voltage sensor and a current sensor are proposed with recursive least-square (RLS) and unscented Kalman filter (UKF) algorithms. The fault diagnosis scheme uses an open-circuit voltage residual generator and a capacity residual generator to generate multiple residuals. In view of the different applicable state of charge (SOC) intervals of each residual, different residuals need to be selected according to the different SOC intervals to evaluate whether a sensor fault occurs during residual evaluation. The fault values of the voltage and current sensors are derived in detail based on the open-circuit voltage residual and the capacity residual, respectively, and applied to the fault-tolerant control of battery parameters and state estimations. The performance of the proposed approaches is demonstrated and evaluated by simulations with MATLAB and experimental studies with a commercial lithium-ion battery cell.

Keywords: battery management system; sensor fault diagnosis; fault-tolerant control; state of charge; open-circuit voltage; multiple residuals



Citation: Yu, Q.; Wan, C.; Li, J.; Xiong, R.; Chen, Z. A Model-Based Sensor Fault Diagnosis Scheme for Batteries in Electric Vehicles. *Energies* **2021**, *14*, 829. <https://doi.org/10.3390/en14040829>

Academic Editor: Frede Blaabjerg
Received: 20 January 2021
Accepted: 3 February 2021
Published: 5 February 2021

Publisher's Note: MDPI stays neutral with regard to jurisdictional claims in published maps and institutional affiliations.



Copyright: © 2021 by the authors. Licensee MDPI, Basel, Switzerland. This article is an open access article distributed under the terms and conditions of the Creative Commons Attribution (CC BY) license (<https://creativecommons.org/licenses/by/4.0/>).

1. Introduction

The development of electric vehicles (EVs) is the consensus of all countries in the world to deal with the energy crisis and environmental deterioration. Lithium-ion batteries are currently the first choice for battery systems due to their excellent performance, but given the limitations of their cell voltage and energy density, EVs are often equipped with hundreds of battery cells [1]. Therefore, an appropriate battery management system (BMS) is indispensable for the safe and reliable operation of battery systems [2]. A BMS has many functions; however, most researchers focus on the estimation of the state of charge (SOC) [3–5] and state of health (SOH) [6–8], and little attention has been paid to fault diagnosis techniques until the occurrence of several accidents related to battery systems in EVs in recent years [9,10]. Internal short-circuit and external short-circuit faults of the battery caused by electrical abuse, electrical abuse, and mechanical abuse were considered to be the main causes of battery system safety accidents [11–15]. The diagnosis of short-circuit faults is basically based on measurement data collected by sensors to establish various diagnostic models and compare the measured values with the predicted values of the models to determine whether a fault has occurred [16,17]. Therefore, the accuracy of collected sensor data directly determines the reliability of the battery fault diagnosis results. In addition, once the acquisition sensor fails, it will affect the realization of other functions that rely on data acquisition in the BMS and further affect the safety of the battery

system [18]. Hence, sensor fault diagnosis is of great importance to ensure the healthy operations of a BMS.

Sensor fault diagnosis methods are basically divided into hardware redundancy methods and software redundancy methods. The former realizes sensor fault detection and isolation by increasing the number of acquisition sensors or changing the topology arrangement of acquisition sensors [19]. The latter includes model-based methods, machine-learning-based methods, and expert-system-based methods. Among them, the model-based method is the most widely used method in the literature [20], the basic idea of which is to reconstruct the fault model and compare the predicted value of the model with the measured value or reference value to determine whether a fault has occurred [21,22]. In other words, the fault diagnosis process of this method includes two steps: residual generation and residual evaluation. Liu et al. [23] take the difference between the predicted voltage of an equivalent circuit model and the measured value of a voltage sensor as the residual and judge whether a sensor fault occurred by comparing the cumulative sum of the residual and predetermined threshold, and then the structured residual method is used to effectively isolate the sensor fault [24]. The difficulty of determining the threshold is the shortcoming of the sensor fault diagnosis method using the voltage prediction error. Dey et al. [25] compare the predicted and measured values of temperature, current, and voltage based on the electrical–thermal coupling model and the sliding mode observer (SMO), respectively, to construct three residuals to achieve sensor fault detection and isolation. Biron et al. [26] also use an electrical–thermal coupling model to generate temperature, current, and voltage residuals to achieve sensor fault detection and isolation, but the residual generation process uses a Kalman filter (KF) and SMO. The problem with the need to construct a current residual generator for the fault diagnosis method is that it is very difficult and complicated to obtain the estimated value of the current that is often used as the model input. To address this issue, Ablay et al. [27] use an electrical–thermal coupling model and observer to generate residuals of temperature, voltage, and resistance for sensor fault detection and isolation. Although the battery dynamic characteristic parameter such as resistance is different in sensor fault and fault-free conditions, it is difficult to obtain the reference resistance in the case of a sensor fault because it is easily affected by the current rate and SOC interval. Therefore, it cannot be directly applied to the sensor fault diagnosis of the battery system. In fact, not only do the dynamic characteristic parameters change when the sensor fails but the various states of the battery also deviate from the expected values [28,29]. Therefore, Xu et al. [30] use the state of energy (SOE) estimation error as the residual to detect a current sensor fault. In addition, the errors of the estimated SOC and capacity are treated as the residuals to detect and isolate the current and voltage sensors' faults in our previous work [31]. Although the calculation of the estimation errors of SOC and SOE is relatively fast, it takes a relatively long time to detect and isolate sensor faults. On the other hand, the method with a capacity error can realize sensor fault diagnosis in a relatively short time, but it cannot be applied to the initial stage of discharge due to limitations [31].

In fact, the fault-tolerant control should be carried out after fault detection and isolation to reduce potential safety hazards [32,33]. However, most studies are satisfied with the detection and isolation of sensor fault, and very little work is documented in the literature on sensor fault-tolerant control in battery systems. Xu et al. [30] add the current sensor fault into a state vector and then realize the online identification and fault-tolerant control of a current sensor fault through the proportional integral observer (PIO). Zhao et al. [34] solve this issue by including a sensor fault into a state vector and reformulating the model to achieve current and voltage sensors' fault-tolerant control with the unscented KF (UKF) algorithm. In their studies, the initial value of the sensor fault in the state vector is set to 0. In fact, it takes a lot of time to retune the measurement noise and system noise of the UKF algorithm for the augmented model. Although the augmented model can realize the fault-tolerant control of the battery state, it ignores the fault-tolerant control of the parameter identification process. In addition, it takes a long time for the estimated value of

the sensor fault to converge from the initial value of 0 to the true value. Except for methods based on augmented models, almost no works in the literature have been found to discuss how to estimate sensor fault values.

In order to solve the aforementioned issues, a model-based sensor fault diagnosis scheme is proposed for battery systems in EVs. The main innovations are as follows:

- A model-based sensor fault diagnosis method with parameter residual and state residuals is proposed. The estimation error of the battery static characteristic parameter, i.e., the open-circuit voltage (OCV), is used as a residual for sensor fault diagnosis, which only has a good effect in the beginning and middle stages of the charging and discharging process. The estimated capacity derived from the ratio of the accumulated charge to the SOC difference at various nonadjacent sampling times is used to generate state residuals to detect the sensor fault. These residuals are only suitable for sensor fault diagnosis in the middle and late stages of the charging and discharging process. In view of the different application intervals of the two residuals, a sensor fault diagnosis scheme with two kinds of residuals is proposed.
- A fault identification and fault-tolerant control strategy is proposed. The fault values of the voltage sensor and current sensor are derived based on the OCV residual and the capacity residual respectively. Then, the fault value is applied to the parameter identification and state estimation of the battery for fault-tolerant control to ensure the safety of the battery.

The remainder of this paper is organized as follows. Section 2 develops the battery model. Section 3 introduces the sensor fault detection and isolation scheme. Section 4 carries out the sensor fault-tolerant control. Section 5 establishes simulation and experimental validation. Conclusions are finally given in Section 6.

2. Battery Model

The battery model adopted here is the first-order resistor-capacitor model depicted in Figure 1, which includes an OCV that is a nonlinear function of SOC [35,36], an ohmic resistance R_o , and resistor-capacitor (R_p – C_p) elements that reflect the dynamics of the batteries. I represents the battery charge/discharge current, and U_p and U_t denote the battery polarization voltage and terminal voltage, respectively.

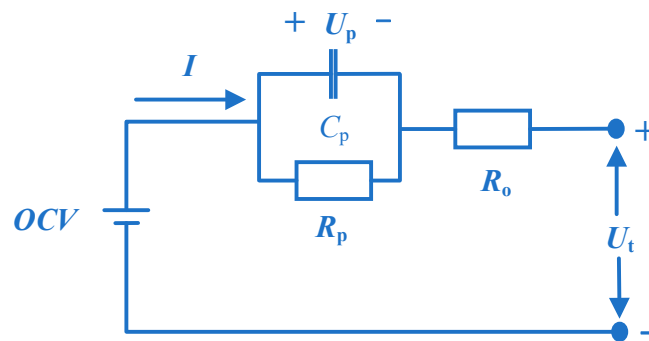


Figure 1. First-order resistor-capacitor battery model.

The electrical dynamics of this battery model can be written as

$$\begin{cases} U_{t,k} = OCV_k - U_{p,k} - I_k R_{o,k} \\ U_{p,k+1} = \exp(-\Delta t/\tau_k) U_{p,k} + (1 - \exp(-\Delta t/\tau_k)) R_{p,k} I_k \end{cases}, \text{define: } \tau_k = R_{p,k} C_{p,k} \quad (1)$$

The battery OCV is generally modeled as a nonlinear function of SOC [36]

$$\begin{cases} OCV_k = k_1 z_k + k_2 z_k^2 + k_3 z_k^3 + k_4/z_k + k_5 \ln(z_k) + k_6 \ln(1 - z_k) \\ z_k = z_{k-1} - \eta I_k \Delta t / Q \end{cases} \quad (2)$$

where k_1-k_6 are the fitting coefficients of the OCV model, z represents the battery SOC, η is the coulomb efficiency, Δt is the sampling interval, and Q denotes the maximum available capacity of the battery cell.

When the acquisition sensor is faulty, the sensor measurements can be expressed as

$$\begin{cases} I_m = I + I_f \\ U_{t,m} = U_t + U_f \end{cases} \quad (3)$$

where I_m and $U_{t,m}$ are measured variables, and I_f and U_f are the current and voltage faults, respectively. It is assumed that I_f and U_f are bounded by the finite values, and only one sensor fault can occur at the same time.

3. Sensor Fault Detection

In this section, we mainly focus on the sensor fault detection with the multiple residuals scheme. The sensor fault isolation methods in the battery system are discussed in [31]. The proposed sensor fault diagnosis scheme is depicted in Figure 2. In the following paragraphs, the specific elements of the scheme are described in detail.

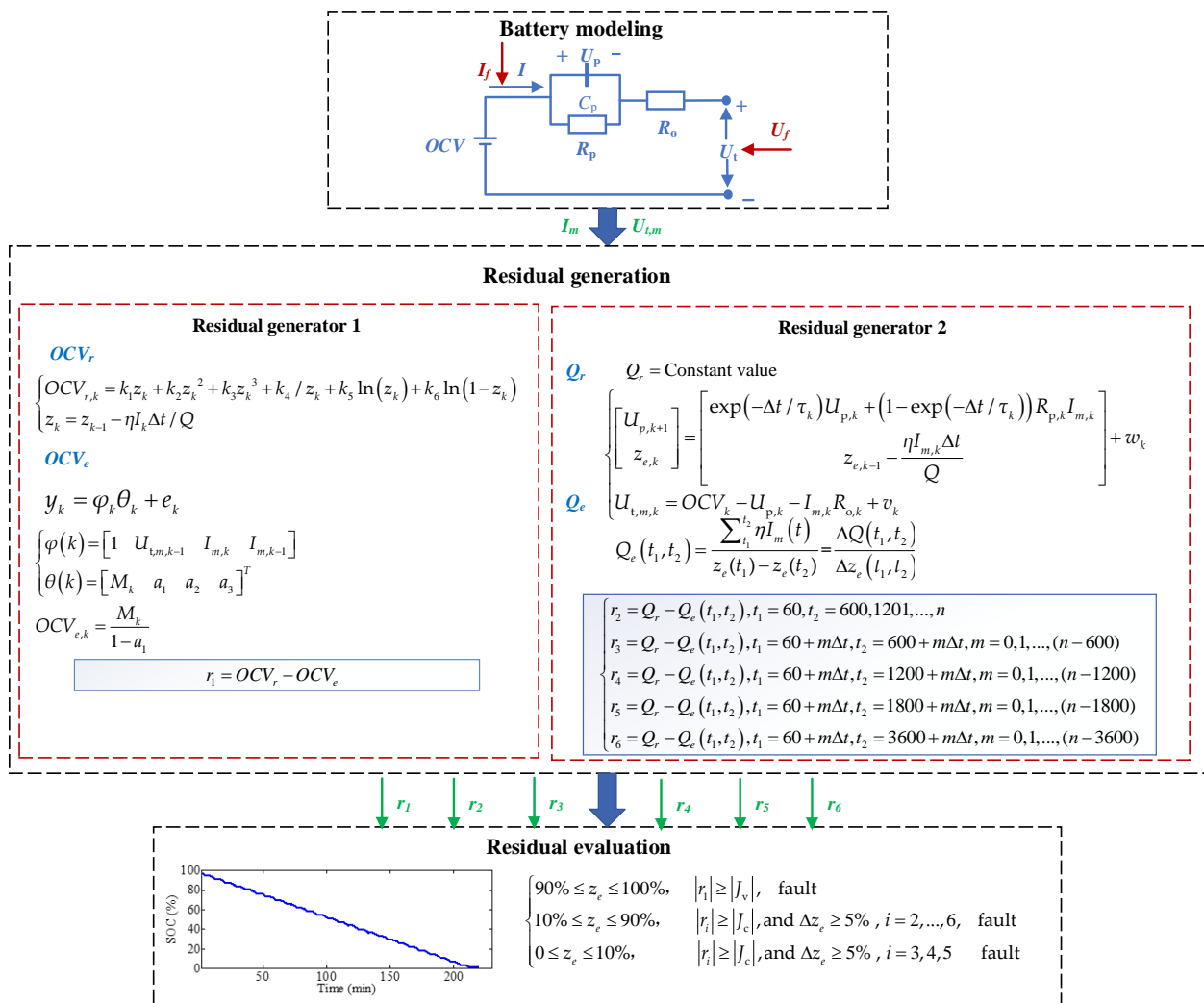


Figure 2. Sensor fault diagnosis scheme.

3.1. Residual Generator 1

In order to obtain higher model accuracy in a BMS, offline identification methods have been gradually replaced by online parameter identification methods. When parameter identification is performed by RLS [37] and nonlinear Kalman filters [38], the dynamic characteristic parameters of the battery change with the current rate and SOC interval during the discharge process, so it is difficult to obtain the reference value of the dynamic characteristic parameters when the sensor fails to generate the residual. In fact, the battery static characteristic parameter (i.e., OCV) can also be estimated by an online identification method [39], and its reference value can also be calculated by Equation (2) at the whole discharge process. Therefore, the residual r_1 can be defined as

$$r_1 = OCV_r - OCV_e \quad (4)$$

where the reference value OCV_r is calculated via Equation (2), and the estimated OCV_e is obtained by the online identification method.

RLS is a widely used optimization algorithm in battery parameters identification. For a system shown in Equation (5), parameters can be iteratively updated with RLS [39].

$$y_k = \varphi_k \theta_k + e_k \quad (5)$$

where y_k is system output, φ_k is the coefficient vector, θ_k is the parameter vector, and e_k is the terminal voltage prediction error.

For the lithium-ion battery model, the terminal voltage $U_{t,m,k}$ is usually regarded as the output y_k , φ_k , and θ_k can be defined as

$$\begin{cases} \varphi(k) = [1 & U_{t,m,k-1} & I_{m,k} & I_{m,k-1}] \\ \theta(k) = [M_k & a_1 & a_2 & a_3]^T \end{cases} \quad (6)$$

M_k , a_1 , a_2 , and a_3 are the transformation quantities when the nonlinear Equation (1) is linearized, which can be expressed as

$$\begin{cases} M_k = OCV_e - a_1 OCV_e \\ a_1 = -\frac{\Delta t - 2R_p C_p}{\Delta t + 2R_p C_p} \\ a_2 = -\frac{R_o \Delta t + R_p \Delta t + 2R_o R_p C_p}{\Delta t + 2R_p C_p} \\ a_3 = -\frac{R_o \Delta t + R_p \Delta t - 2R_o R_p C_p}{\Delta t + 2R_p C_p} \end{cases} \quad (7)$$

Therefore, when the θ_k at each sampling moment is identified by RLS, the estimated value of OCV_e can be further obtained:

$$OCV_{e,k} = \frac{M_k}{1 - a_1} \quad (8)$$

Then, the residual r_1 can be calculated at the whole discharge process. It should be noted that the estimation error of OCV is smaller in the middle and high SOC intervals and larger in the low SOC interval [39], which may cause false alarms in the low SOC interval.

3.2. Residual Generator 2

Once the sensor fails, the predicted voltage based on the Kalman filters for state estimation has a good followability with the actual measured voltage, but the sensor fault will cause the estimated states to deviate from the accurate values. Therefore, changes in states such as SOE [30], SOC [31], and capacity (an index of battery health) [31] can be used for sensor fault diagnosis. Considering that it takes a long time to diagnose sensor

faults with changes in SOC and SOE, the estimated capacity error shown in Equation (9) is selected to diagnose sensor faults.

$$r_2 = Q_r - Q_e \quad (9)$$

where the reference capacity Q_r is a constant value in one charge and discharge cycle, which can be determined as the average value of the estimated capacity Q_e of the previous charge and discharge cycle. The estimated capacity Q_e is calculated by

$$Q_e(t_1, t_2) = \frac{\sum_{t_1}^{t_2} \eta I_m(t)}{z_e(t_1) - z_e(t_2)} = \frac{\Delta Q(t_1, t_2)}{\Delta z_e(t_1, t_2)} \quad (10)$$

where t_1 and t_2 are two values of k at two different sampling times, and $z_e(t_1)$ and $z_e(t_2)$ are estimated SOC values based on the UKF algorithm.

The lithium-ion battery model can also be transformed to the state-space equation

$$\begin{cases} \begin{bmatrix} U_{p,k+1} \\ z_{e,k} \end{bmatrix} = \begin{bmatrix} \exp(-\Delta t/\tau_k)U_{p,k} + (1 - \exp(-\Delta t/\tau_k))R_{p,k}I_{m,k} \\ z_{e,k-1} - \frac{\eta I_{m,k}\Delta t}{Q} \end{bmatrix} + w_k \\ U_{t,m,k} = OCV_k - U_{p,k} - I_{m,k}R_{o,k} + v_k \end{cases} \quad (11)$$

where w and v are the process noise and measurement noise. Note that capacity Q here is a constant value, which is determined as the average value of the estimated capacity Q_e of the previous charge and discharge cycle. OCV_k here is the value obtained by substituting $z_{e,k}$ estimated by UKF into the OCV model.

The specific process of updating the battery state $z_{e,k}$ in Equation (11) according to the UKF algorithm can be found in our previous study [31]. Then, the estimated capacity Q_e can be derived from Equation (10). It should be pointed out that there are two issues in directly using Equations (14)–(16) for sensor fault diagnosis. Since the capacity is the ratio of the amount of charge accumulated over a period of time to the change in SOC, Equation (10) does not apply to the initial stage of battery discharge (i.e., high SOC interval) [31]. In addition, the estimation accuracy of capacity is closely related to the selection of t_1 and t_2 . The more electricity is discharged between t_1 and t_2 , the smaller the estimation error of capacity, but the higher the missed alarm rate of fault diagnosis. Conversely, the less electricity is discharged between t_1 and t_2 , the larger the estimation error of capacity, and the higher the false alarm rate of fault diagnosis. After many trials, we suggest that the selection and determination of t_1 and t_2 should be based on whether the SOC difference between these two times is more than 5%. In view of the unpredictability of the current rate during the battery discharge, multiple groups of t_1 and t_2 are selected to generate capacity residuals to participate in sensor fault diagnosis. The diagnosis process needs to judge and eliminate residuals with SOC differences of less than 5%. Assuming that the entire discharge process needs to collect n sets of data and the sampling interval is Δt , the capacity residuals can be defined as follows

$$\begin{cases} r_2 = Q_r - Q_e(t_1, t_2), t_1 = 60, t_2 = 600, 1201, \dots, n \\ r_3 = Q_r - Q_e(t_1, t_2), t_1 = 60 + m\Delta t, t_2 = 600 + m\Delta t, m = 0, 1, \dots, (n - 600) \\ r_4 = Q_r - Q_e(t_1, t_2), t_1 = 60 + m\Delta t, t_2 = 1200 + m\Delta t, m = 0, 1, \dots, (n - 1200) \\ r_5 = Q_r - Q_e(t_1, t_2), t_1 = 60 + m\Delta t, t_2 = 1800 + m\Delta t, m = 0, 1, \dots, (n - 1800) \\ r_6 = Q_r - Q_e(t_1, t_2), t_1 = 60 + m\Delta t, t_2 = 3600 + m\Delta t, m = 0, 1, \dots, (n - 3600) \end{cases} \quad (12)$$

where t_1 starts from 60 instead of 1 because it takes into account the convergence process of the algorithm during state estimation.

3.3. Residual Evaluation

In view of the different applicable SOC intervals of each residual in the battery discharge process, it is necessary to select different residuals according to the SOC interval as follows to determine whether a fault has occurred during residual evaluation.

$$\begin{cases} 90\% \leq z_e \leq 100\%, & |r_1| \geq |J_v|, \text{ fault} \\ 10\% \leq z_e \leq 90\%, & |r_i| \geq |J_c|, \text{ and } \Delta z_e \geq 5\%, i = 2, \dots, 6, \text{ fault} \\ 0 \leq z_e \leq 10\%, & |r_i| \geq |J_c|, \text{ and } \Delta z_e \geq 5\%, i = 3, 4, 5 \text{ fault} \end{cases} \quad (13)$$

where J_v and J_c are the thresholds for OCV residual and capacity residuals, respectively. The threshold J directly determines the false alarm rate and missed alarm rate of fault diagnosis. Based on experience, J_v and J_c are defined as 0.1 V and 0.1 Ah, respectively, in this study.

4. Sensor Fault-Tolerant Control Strategy

4.1. Voltage Sensor Fault Identification and Tolerant Control

Active fault-tolerant control after fault detection is of great significance for improving the safety of battery systems, and the accurate fault identification value is the basis for fault-tolerant control. In this section, we propose a new method for determining the values of a sensor fault to improve the effect of fault tolerance.

For voltage sensor faults, the parameters related to the voltage sensor fault value U_f will be derived from the perspective of parameters identification based on the RLS algorithm.

When a voltage sensor fault occurs, the battery terminal voltage $U_{t,m}$ will be transformed into

$$U_{t,m,k} = U_{f,k} + OCV_{e,k} - a_1 OCV_{e,k} + a_1 U_{t,m,k-1} + a_2 I_{m,k} + a_3 I_{m,k-1} \quad (14)$$

When the value of U_f is not known, the coefficient vector φ_k and parameter vector θ_k are still defined according to Equation (6), M_k actually represents

$$M_k = U_{f,k} + OCV_{e,k} - a_1 OCV_{e,k} \quad (15)$$

The estimated OCV_e is

$$OCV_{e,k} = \frac{M_k}{1 - a_1} - \frac{U_{f,k}}{1 - a_1} \quad (16)$$

Since only the voltage sensor fails, the reference OCV_r has not changed, so the residual r_1 is

$$r_{1,k} = OCV_{r,k} - \frac{M_k}{1 - a_1} + \frac{U_{f,k}}{1 - a_1} \quad (17)$$

When a voltage sensor fault occurs, a_2 and a_3 are the coefficients of the current. Their changes can be basically ignored. The main parameters that change are M_k and a_1 , but as the sampling time increases, M_k and a_1 also tend to stabilize, then $OCV_{r,k} = \frac{M_k}{1 - a_1}$, and Equation (18) can be simplified as

$$U_{f,k} = (1 - a_1)r_{1,k} \quad (18)$$

Since the voltage sensor fault threshold J_v is less than the sensor fault U_f , the value of r_1 just exceeding the threshold J_v cannot be regarded as the fault value U_f . Instead, after r_1 exceeds the threshold J_v , it will quickly reach a stable value and fluctuate around this value. The average value of the fluctuation value can be regarded as a voltage sensor fault U_f for fault-tolerant control. The mathematical expression is as follows

$$U_f \approx \frac{\sum_{t_b}^{t_a} (1 - a_1) r_{1,k}}{(t_b - t_a) / \Delta t + 1} \quad (19)$$

where t_a is the starting time when r_1 reaches a stable value, and t_b is the time when r_1 reaches and keeps a stable value for a certain period of time.

After the fault value U_f is obtained, parameter identification and state estimation can be fault tolerant by Equations (14) and (20), respectively.

$$\begin{cases} \begin{bmatrix} U_{p,k+1} \\ z_{e,k} \end{bmatrix} = \begin{bmatrix} \exp(-\Delta t / \tau_k) U_{p,k} + (1 - \exp(-\Delta t / \tau_k)) R_{p,k} I_{m,k} \\ z_{e,k-1} - \eta I_{m,k} \Delta t / Q \end{bmatrix} + w_k \\ U_{t,m,k} = U_{f,k} + OC V_k - U_{p,k} - I_{m,k} R_{o,k} + v_k \end{cases} \quad (20)$$

4.2. Current Sensor Fault Identification and Tolerant Control

When a current sensor fault occurs, we derive the current sensor fault value I_f from the perspective of capacity residual generation. Equations (9) and (10) can be transformed into

$$r(t_1, t_2) = Q_r - \frac{\sum_{t_1}^{t_2} \eta I_m(t)}{z_e(t_2) - z_e(t_1)}, r(t_3, t_4) = Q_r - \frac{\sum_{t_3}^{t_4} \eta I_m(t)}{z_e(t_3) - z_e(t_4)} \quad (21)$$

where $r(t_1, t_2)$ is the capacity residual from t_1 to t_2 when there is no current sensor fault, and $r(t_3, t_4)$ is the capacity residual from t_3 to t_4 when a current sensor fault occurs. The selection of t_1 and t_2 is based on the fact that the SOC change during this period is equal to the SOC change during the t_3 and t_4 period, i.e., $z_e(t_3) - z_e(t_4) = z_e(t_1) - z_e(t_2)$. Then, according to Equation (21), the value of the current sensor fault I_f can be derived as follows

$$\begin{aligned} r(t_3, t_4) - r(t_1, t_2) &= \frac{\sum_{t_3}^{t_4} \eta I_f(t) - \sum_{t_3}^{t_4} \eta I_m(t) + \sum_{t_1}^{t_2} \eta I_m(t)}{z_e(t_1) - z_e(t_2)} \\ \Rightarrow \sum_{t_3}^{t_4} \eta I_f(t) &= (r(t_3, t_4) - r(t_2, t_1))(z_e(t_1) - z_e(t_2)) + \sum_{t_3}^{t_4} \eta I_m(t) - \sum_{t_1}^{t_2} \eta I_m(t) \end{aligned} \quad (22)$$

When the current sensor fault I_f is obtained, the fault-tolerant control of the battery parameters and states is carried out as follows:

$$U_{t,m,k} = OC V_{e,k} - a_1 OC V_{e,k} + a_1 U_{t,k-1} + a_2 (I_{m,k} - I_f) + a_3 (I_{m,k-1} - I_f) \quad (23)$$

$$\begin{cases} \begin{bmatrix} U_{p,k+1} \\ z_{e,k} \end{bmatrix} = \begin{bmatrix} \exp(-\Delta t / \tau_k) U_{p,k} + (1 - \exp(-\Delta t / \tau_k)) R_{p,k} (I_{m,k} - I_f) \\ z_{e,k-1} - \frac{\eta (I_{m,k} - I_f) \Delta t}{Q} \end{bmatrix} + w_k \\ U_{t,m,k} = OC V_k - U_{p,k} - (I_{m,k} - I_f) R_{o,k} + v_k \end{cases} \quad (24)$$

When a sensor fault occurs, Equations (19) and (22) can be used to quickly obtain the fault values and avoid the difficulty in retuning the parameters required to build the augmented model. The process of fault identification and fault-tolerant control is summarized as shown in Figure 3.

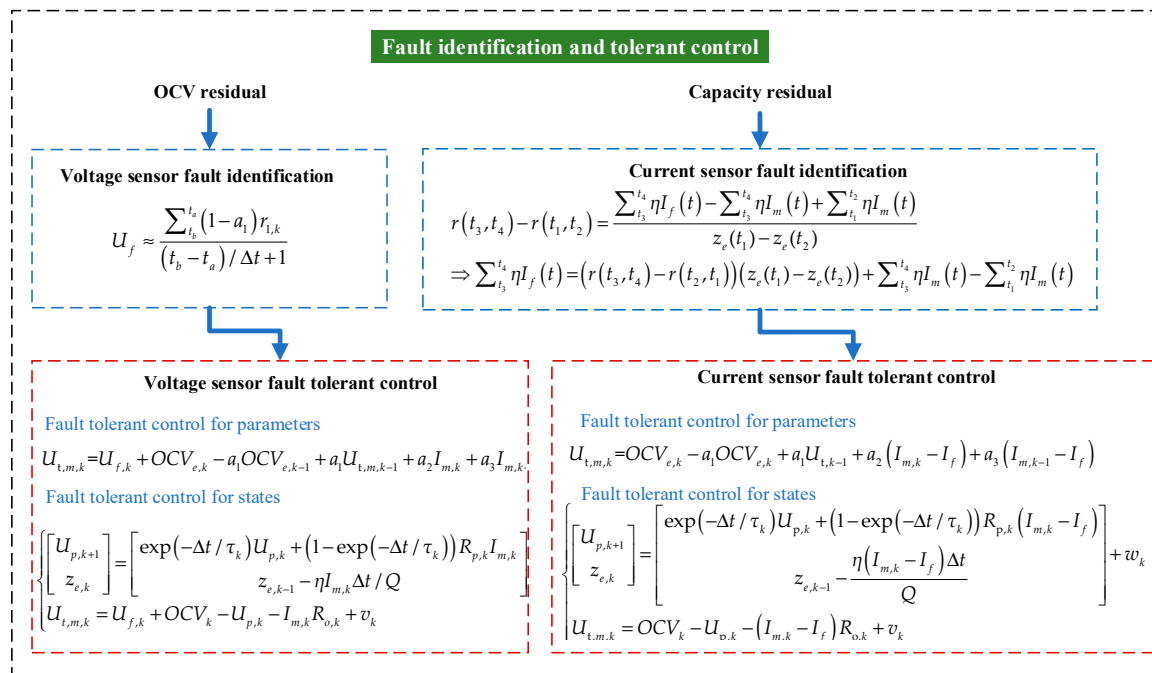


Figure 3. Sensor fault identification and tolerant control.

5. Verification and Discussion

5.1. Experiments

The effectiveness of the proposed diagnosis scheme and fault-tolerant control strategy was verified by conducting experimental tests and simulating studies on a LiNiMnCoO₂ cell. The rated capacity and voltage are 2.1 Ah and 3.6 V, respectively. The dynamic stress test (DST) data when the sensors have no faults, that is, the current and voltage profiles, are shown in Figure 4. The corresponding reference SOC in the sensor fault-free condition is illustrated in Figure 5. To simulate the voltage sensor fault and current sensor fault, a voltage of 0.25 V and a current of 0.25 A were injected into the voltage and current profiles shown in Figure 4, respectively.

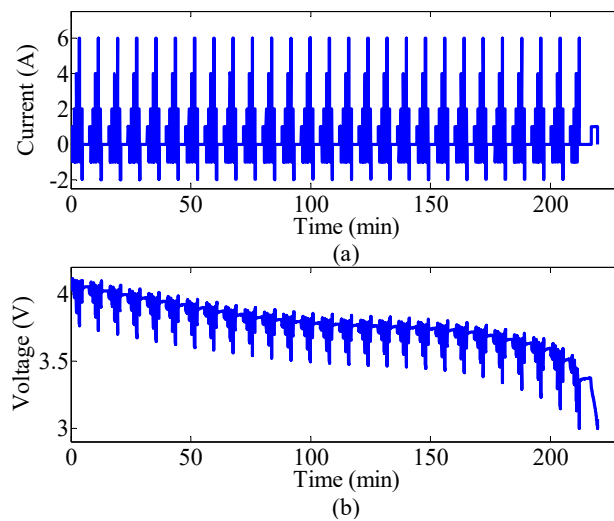


Figure 4. Dynamic stress test (DST) test at 25 °C in the sensor fault-free condition: (a) current profile; (b) voltage profile.

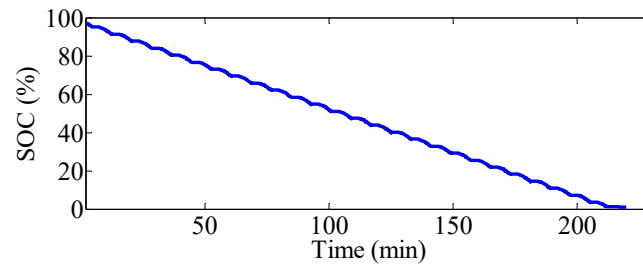


Figure 5. Reference state of charge (SOC) in the sensor fault-free condition.

5.2. Sensor Fault Detection

In the absence of a sensor fault, the residuals based on OCV and capacity are shown in Figures 6 and 7. The absolute value of residual r_1 remains within 0.1 V in the 10–100% SOC interval and exceeds 0.1 V in the 0–10% SOC interval. That is to say, the residual r_1 has a higher false alarm rate in the low SOC interval and is more suitable for fault diagnosis in the middle and high SOC intervals. As for the capacity residuals that cannot be used at the beginning of discharge, the residuals obtained by different t_1 and t_2 have different effects in the discharge process. The residual r_2 is relatively smooth and stable throughout the discharge process, which is very close to the reference capacity Q_r , but the missed alarm rate is higher in the later stage of the discharge. r_3 is the capacity residual obtained by continuously calculating the data of 600 sampling points (that is, the SOC change is less than 5%) during the discharge process. The maximum value exceeds 0.1 Ah in the low SOC interval, which means the false alarm rate is higher in the low SOC range. r_4 , r_5 , and r_6 are the capacity residuals calculated according to Equation (12) using the data of 1200, 1800, and 3600 sampling points during the discharge process. The SOC change in these residuals exceeds 5%. Note that the smaller the SOC change, the greater the residual value in the low SOC interval, which also means higher sensitivity to a sensor fault. Therefore, for the dynamic operating conditions shown in Figure 4, the residual r_1 participates in the sensor fault diagnosis in the high and middle SOC intervals, the residuals of r_2 and r_3 only participate in the sensor fault diagnosis in the middle SOC interval, and r_4 , r_5 , and r_6 participate in both the middle and low SOC intervals.

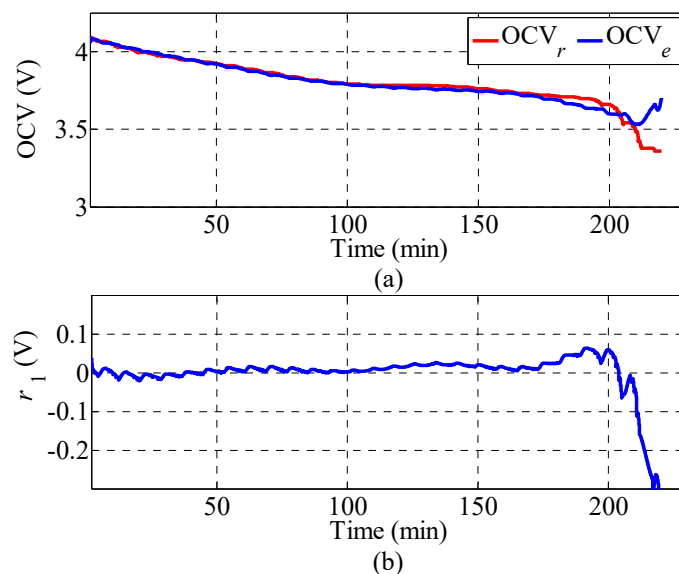


Figure 6. Estimated open-circuit voltage (OCV) and the residual r_1 : (a) OCV; (b) r_1 .

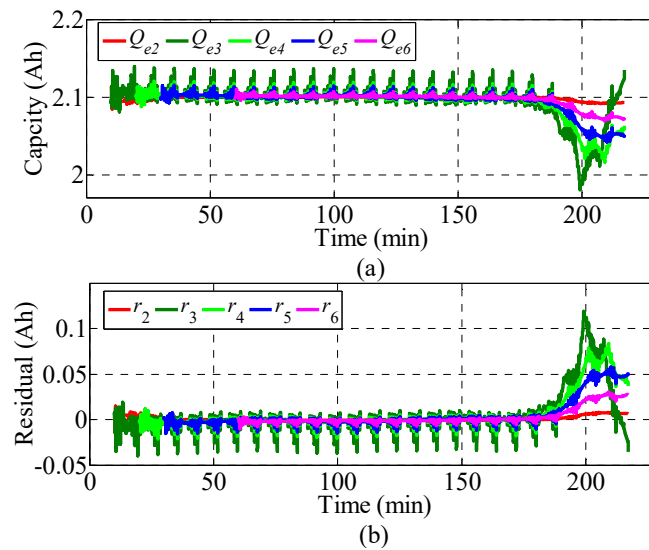


Figure 7. Estimated capacity and capacity residuals: (a) capacity; (b) r_2 , r_3 , r_4 , r_5 , and r_6 .

Residual responses for when a voltage sensor fault occurred at the 50th minute are illustrated in Figure 8. r_1 exceeds the threshold J_v in 51.1 min, rises rapidly to 0.245 V, and then fluctuates around 0.25 V until the battery is discharged to 10% SOC. r_3 exceeds the threshold J_c in 54.5 min, followed by r_4 , r_5 , r_6 , and r_2 , which is consistent with our expectation that the smaller the SOC change, the higher the sensitivity to a sensor fault. In addition, it can be seen that the OCV residual takes a shorter time to detect the voltage sensor fault than the capacity residuals.

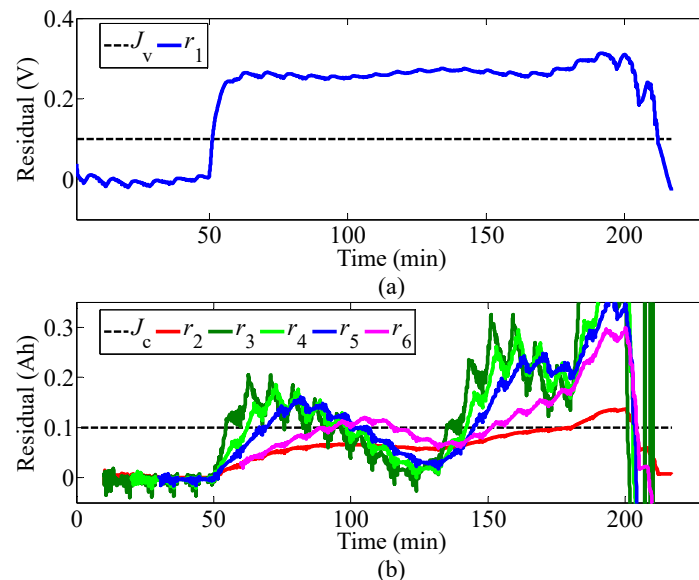


Figure 8. Residual responses for a voltage sensor fault: (a) r_1 ; (b) r_2 , r_3 , r_4 , r_5 , and r_6 .

Residual responses for a current sensor fault occurring at the 50th minute are shown in Figure 9. r_1 increases slowly after the current sensor fault occurs, exceeds the threshold J_v at 72.4 min, and continues to increase slowly. Similar to the occurrence of a voltage sensor fault, among the five capacity residuals, r_3 with a relatively smaller SOC change is still the first to exceed the threshold J_c at 62.4 min. However, unlike the voltage sensor fault diagnosis, the capacity residuals take a shorter time to detect the current sensor fault than the OCV residual.

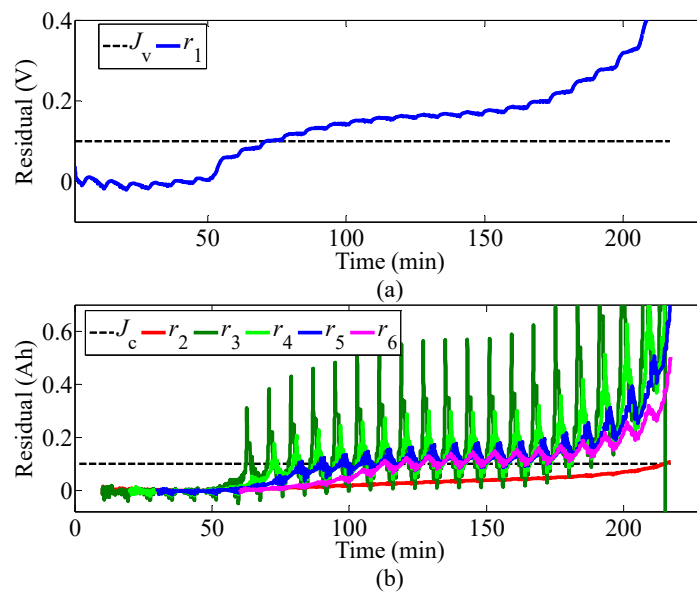


Figure 9. Residual responses for a current sensor fault: (a) r_1 ; (b) r_2 , r_3 , r_4 , r_5 , and r_6 .

Since the voltage and current sensor faults are first detected through r_1 and r_3 shown in Figure 10, the sensor fault values can be calculated by Equations (19) and (22), respectively. For the voltage sensor fault, t_a and t_b are 56.3 min and 61.3 min, respectively, the average value of the voltage sensor fault U_f is 0.247 V, and the fault error is 0.003 V. If t_b is farther from t_a , the fault value U_f may be more accurate, but it will cause the later time to start fault-tolerant control. Therefore, this study chooses the mean value of the residual r_1 within 5 min as the fault value. Figure 11a shows the fault-tolerant control process of battery parameter identification. The battery static characteristic parameter OCV is automatically corrected to the reference value from 61.3 min based on the voltage fault value and the SOC difference caused by the fault.

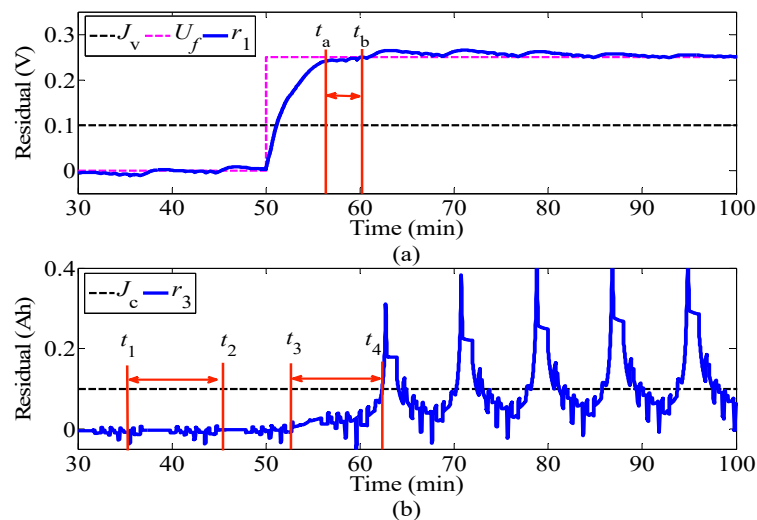


Figure 10. Residual responses for sensor faults: (a) r_1 for a voltage sensor fault; (b) r_3 for a current sensor fault.

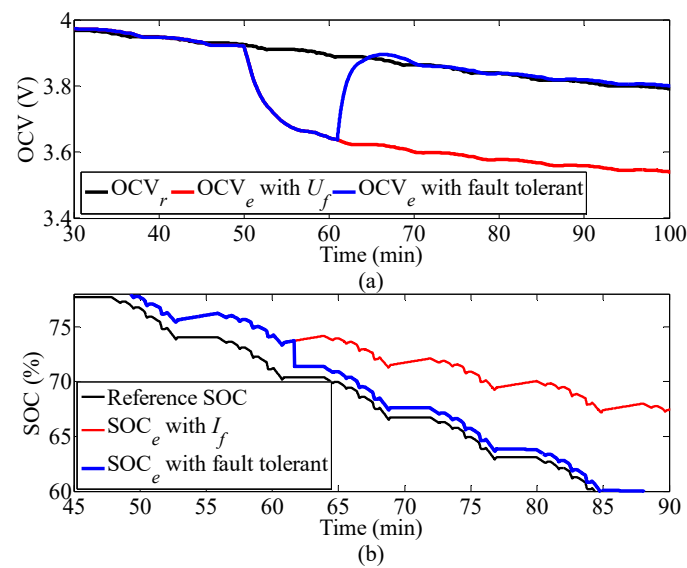


Figure 11. Fault-tolerant control for parameter identification and state estimation: (a) OCV; (b) SOC.

For the current sensor fault, the time when r_3 reaches the threshold J_c is selected as t_4 , namely 62.4 min, t_3 is set to be 10 min forward from t_4 , the SOC change between t_3 and t_4 is calculated, and t_1 and t_2 are selected when the sensor does not fail. The selection of t_1 and t_2 is based on the fact that the SOC change during this period is equal to the SOC change during the t_3 and t_4 period. Then, according to Equation (22), the fault value of the current sensor I_f is set to 0.245 A, and the error is 0.005 A. Figure 11b shows the fault-tolerant control process of battery state estimation. The battery SOC is automatically corrected to the reference value based on the current fault value and the SOC difference caused by the fault from 62.4 min.

6. Conclusions

In this paper, a hybrid sensor fault diagnosis scheme and fault-tolerant control strategy are proposed. The hybrid fault diagnosis scheme realizes the diagnosis of a current sensor fault and voltage sensor fault by calculating multiple OCV and capacity residuals in parallel. Further, the sensor fault values are derived by postprocessing the residuals applied to the fault-tolerant control of parameter identification and state estimation. Finally, simulations and experimental studies were conducted in a commercial NMC lithium-ion battery cell to verify the fault diagnosis scheme and fault control strategy. One shortcoming of this method is that it is only suitable for faster sampling frequencies and not suitable for operating conditions with large sampling intervals. Taking into account the number of calculations, this study chose five capacity residuals. In view of the different sensitivity of different residuals to faults, selecting the appropriate capacity residuals to meet complex vehicle practical application conditions is the focus of our future research.

Author Contributions: Conceptualization, C.W. and Z.C.; methodology, Q.Y.; validation, Z.C., and J.L.; formal analysis, R.X.; writing—original draft preparation, Q.Y.; writing—review and editing, R.X.; All authors have read and agreed to the published version of the manuscript.

Funding: This work has been supported by the Shandong Provincial Natural Science Foundation Project (ZR2020ME209) and the National Natural Science Foundation of China (Grant No. 51977029).

Institutional Review Board Statement: Not applicable.

Informed Consent Statement: Not applicable.

Data Availability Statement: Data sharing not applicable.

Acknowledgments: The systemic experiments of the lithium-ion batteries were performed at the Advanced Energy Storage and Application (AESA) Group, Beijing Institute of Technology.

Conflicts of Interest: The authors declare no conflict of interest. As Rui Xiong, a co-author of this paper, is an associate EIC of Energies, he was blinded to this paper during the review, and the paper is independently handled by other editor.

References

1. Jaguemont, J.; Boulon, L.; Dube, Y. A comprehensive review of lithium-ion batteries used in hybrid and electric vehicles at cold temperatures. *Appl. Energy* **2016**, *164*, 99–114. [[CrossRef](#)]
2. Xing, Y.; Ma, E.W.M.; Tsui, K.-L.; Pecht, M. Battery Management Systems in Electric and Hybrid Vehicles. *Energies* **2011**, *4*, 1840–1857. [[CrossRef](#)]
3. Chen, C.; Xiong, R.; Yang, R.; Shen, W.; Sun, F. State-of-charge estimation of lithium-ion battery using an improved neural network model and extended Kalman filter. *J. Clean. Prod.* **2019**, *234*, 1153–1164. [[CrossRef](#)]
4. Chen, Z.; Zhang, Q.; Lu, J.; Bi, J. Optimization-based method to develop practical driving cycle for application in electric vehicle power management: A case study in Shenyang, China. *Energy* **2019**, *186*, 115766. [[CrossRef](#)]
5. Xiong, R.; Li, L.; Yu, Q.; Jin, Q.; Yang, R. A set membership theory based parameter and state of charge co-estimation method for all-weather batteries. *J. Clean. Prod.* **2020**, *249*, 119380. [[CrossRef](#)]
6. Jiang, Y.; Jiang, J.; Zhang, C.; Zhang, W.; Gao, Y.; Li, N. State of health estimation of second-life LiFePO₄ batteries for energy storage applications. *J. Clean. Prod.* **2018**, *205*, 754–762. [[CrossRef](#)]
7. Berecibar, M.; Garmendia, M.; Gandiaga, I.; Crego, J.; Villarreal, I. State of health estimation algorithm of LiFePO₄ battery packs based on differential voltage curves for battery management system application. *Energy* **2016**, *103*, 784–796. [[CrossRef](#)]
8. Yu, Q.; Xiong, R.; Yang, R.; Pecht, M.G. Online capacity estimation for lithium-ion batteries through joint estimation method. *Appl. Energy* **2019**, *255*, 113817. [[CrossRef](#)]
9. Abada, S.; Marlair, G.; Lecocq, A.; Petit, M.; Sauvant-Moynot, V.; Huet, F. Safety focused modeling of lithium-ion batteries: A review. *J. Power Sources* **2016**, *306*, 178–192. [[CrossRef](#)]
10. Wang, Z.; Hong, J.; Liu, P.; Zhang, L. Voltage fault diagnosis and prognosis of battery systems based on entropy and Z-score for electric vehicles. *Appl. Energy* **2017**, *196*, 289–302. [[CrossRef](#)]
11. Feng, X.; He, X.; Lu, L.; Ouyang, M. Analysis on the Fault Features for Internal Short Circuit Detection Using an Electro-chemical-Thermal Coupled Model. *J. Electrochem. Soc.* **2018**, *165*, A155–A167. [[CrossRef](#)]
12. Yang, R.; Xiong, R.; Shen, W.; Lin, X. Extreme Learning Machine Based Thermal Model for Lithium-ion Batteries of Electric Vehicles under External Short Circuit. *Engineering* **2020**. [[CrossRef](#)]
13. Xia, B.; Shang, Y.; Nguyen, T.; Mi, C. External Short Circuit Fault Diagnosis Based on Supervised Statistical Learning. In *2017 IEEE Transportation Electrification Conference and Expo, Asia-Pacific (ITEC Asia-Pacific)*; IEEE: Piscataway, NJ, USA, 2017; pp. 1–5.
14. Feng, X.; Weng, C.; Ouyang, M.; Sun, J. Online internal short circuit detection for a large format lithium ion battery. *Appl. Energy* **2016**, *161*, 168–180. [[CrossRef](#)]
15. Xiong, Q.; Yu, L.Y. Open circuit voltage and state of charge online estimation for lithium ion batteries. *Energy Procedia* **2017**, *142*, 1902–1907. [[CrossRef](#)]
16. Ouyang, M.; Feng, X.; Han, X.; Lu, L.; Li, Z.; He, X. A dynamic capacity degradation model and its applications considering varying load for a large format Li-ion battery. *Appl. Energy* **2016**, *165*, 48–59. [[CrossRef](#)]
17. Sahraei, E.; Campbell, J.C.; Wierzbicki, T. Modeling and short circuit detection of 18650 Li-ion cells under mechanical abuse conditions. *J. Power Sources* **2012**, *220*, 360–372. [[CrossRef](#)]
18. Lin, X.; Stefanopoulou, A.G. Analytic Bound on Accuracy of Battery State and Parameter Estimation. *J. Electrochem. Soc.* **2015**, *162*, A1879–A1891. [[CrossRef](#)]
19. Xia, B.; Mi, C. A fault-tolerant voltage measurement method for series connected battery packs. *J. Power Sources* **2016**, *308*, 83–96. [[CrossRef](#)]
20. Venkatasubramanian, V.; Rengaswamy, R.; Yin, K.; Kavuri, S.N. A review of process fault detection and diagnosis. *Comput. Chem. Eng.* **2003**, *27*, 293–311. [[CrossRef](#)]
21. Xiong, R.; Yu, Q.; Shen, W. Review on sensors fault diagnosis and fault-tolerant techniques for lithium ion batteries in electric vehicles. In *Proceedings of the 2018 13th IEEE Conference on Industrial Electronics and Applications (ICIEA)*, Wuhan, China, 31 May–2 June 2018.
22. Zheng, C.; Chen, Z.; Huang, D. Fault diagnosis of voltage sensor and current sensor for lithium-ion battery pack using hybrid system modeling and unscented particle filter. *Energy* **2020**, *191*, 116504. [[CrossRef](#)]
23. Liu, Z.; He, H. Model-based Sensor Fault Diagnosis of a Lithium-ion Battery in Electric Vehicles. *Energies* **2015**, *8*, 6509–6527. [[CrossRef](#)]
24. Liu, Z.; He, H. Sensor fault detection and isolation for a lithium-ion battery pack in electric vehicles using adaptive extended Kalman filter. *Appl. Energy* **2017**, *185*, 2033–2044. [[CrossRef](#)]
25. Dey, S.; Mohon, S.; Pisu, P.; Ayalew, B. Sensor Fault Detection, Isolation, and Estimation in Lithium-Ion Batteries. *IEEE Trans. Control. Syst. Technol.* **2016**, *24*, 2141–2149. [[CrossRef](#)]
26. Biron, Z.A.; Pisu, P.; Ayalew, B. Observer-Based Diagnostic Scheme for Lithium-Ion Batteries. In *Proceedings of the ASME 2015 Dynamic Systems and Control Conference*, Columbus, OH, USA, 28–30 October 2015.

27. Ablay, G. An Observer-Based Fault Diagnosis in Battery Systems of Hybrid Vehicles. In Proceedings of the 2013 8th International Conference on Electrical and Electronics Engineering (ELECO), San Francisco, CA, USA, 18–19 May 2013; IEEE: Piscataway, NJ, USA, 2013; Volume 2013, pp. 238–242.
28. Couto, L.D.; Kinnaert, M. Internal and Sensor Fault Detection and Isolation for Li-ion Batteries. *IFAC-PapersOnLine* **2018**, *51*, 1431–1438. [[CrossRef](#)]
29. Yu, Q.; Xiong, R.; Lin, C. Model-Based Sensor Fault Detection for Lithium-Ion Batteries in Electric Vehicles. In *2019 IEEE 89th Vehicular Technology Conference (VTC2019-Spring)*; Institute of Electrical and Electronics Engineers (IEEE): Piscataway, NJ, USA, 2019; pp. 1–4.
30. Xu, J.; Wang, J.; Li, S.; Cao, B. A Method to Simultaneously Detect the Current Sensor Fault and Estimate the State of Energy for Batteries in Electric Vehicles. *Sensors* **2016**, *16*, 1328. [[CrossRef](#)]
31. Xiong, R.; Yu, Q.; Shen, W.; Lin, C.; Sun, F. A Sensor Fault Diagnosis Method for a Lithium-Ion Battery Pack in Electric Vehicles. *IEEE Trans. Power Electron.* **2019**, *34*, 9709–9718. [[CrossRef](#)]
32. Karimi, S.; Gaillard, A.; Poure, P.; Saadate, S. Current Sensor Fault-Tolerant Control for WECS with DFIG. *IEEE Trans. Ind. Electron.* **2009**, *56*, 4660–4670. [[CrossRef](#)]
33. Bianchi, F.D.; Ocampo-Martinez, C.; Kunusch, C.; Sánchez-Peña, R.S. Fault-tolerant unfalsified control for PEM fuel cell systems. *IEEE Trans. Energy Convers.* **2015**, *30*, 307–315. [[CrossRef](#)]
34. Zhao, S.; Duncan, S.R.; Howey, D.A. Observability Analysis and State Estimation of Lithium-Ion Batteries in the Presence of Sensor Biases. *IEEE Trans. Control. Syst. Technol.* **2016**, *25*, 326–333. [[CrossRef](#)]
35. Xiong, R.; Yu, Q.; Wang, L.Y.; Lin, C. A novel method to obtain the open circuit voltage for the state of charge of lithium ion batteries in electric vehicles by using H infinity filter. *Appl. Energy* **2017**, *207*, 346–353. [[CrossRef](#)]
36. Yu, Q.-Q.; Xiong, R.; Wang, L.-Y.; Lin, C. A Comparative Study on Open Circuit Voltage Models for Lithium-ion Batteries. *Chin. J. Mech. Eng.* **2018**, *31*, 65. [[CrossRef](#)]
37. Hu, X.; Sun, F.; Zou, Y.; Peng, H. Online estimation of an electric vehicle Lithium-Ion battery using recursive least squares with forgetting. In Proceedings of the 2011 American Control Conference, San Francisco, CA, USA, 29 June–1 July 2011.
38. Yu, Q.; Xiong, R.; Lin, C.; Shen, W.; Deng, J. Lithium-Ion Battery Parameters and State-of-Charge Joint Estimation Based on H-Infinity and Unscented Kalman Filters. *IEEE Trans. Veh. Technol.* **2017**, *66*, 8693–8701. [[CrossRef](#)]
39. Li, Z.; Xiong, R.; Mu, H.; He, H.; Wang, C. A novel parameter and state-of-charge determining method of lithium-ion battery for electric vehicles. *Appl. Energy* **2017**, *207*, 363–371. [[CrossRef](#)]